Polymer 124 (2017) 41–47

Contents lists available at ScienceDirect

Polymer

journal homepage: www.elsevier.com/locate/polymer

Reparation of recycled acrylonitrile- butadiene-styrene by pyromellitic dianhydride: Reparation performance evaluation and property analysis

Yingchun Li [a, *, 1], Xiaolu Wu [a, 1], Jiangfeng Song [b, c], Jianfeng Li [d], Qian Shao [d], Nuo Cao [e], Na Lu [f], Zhanhu Guo [c, **]

[a] School of Materials Science and Engineering, North University of China, Taiyuan 030051, China
[b] School of Science, North University of China, Taiyuan 030051, China
[c] Integrated Composites Laboratory (ICL), Department of Chemical & Biomolecular Engineering, University of Tennessee, Knoxville, TN 37996, USA
[d] College of Chemical and Environmental Engineering, Shandong University of Science and Technology, Qingdao 66590 China
[e] China National Electric Apparatus Research Institute Co., Ltd, Guangzhou, 51000 China
[f] Lyles School of Civil Engineering, School of Materials Engineering, Birck Nanotechnology Center, Purdue University, West Lafayette, IN 47906, USA

ARTICLE INFO

Article history:
Received 31 May 2017
Received in revised form
7 July 2017
Accepted 16 July 2017
Available online 17 July 2017

Keywords:
Recycled ABS
Chain extension
Impact strength

ABSTRACT

The high values of recycled acrylonitrile-butadiene-styrene plastics (rABS) have drawn wide attentions and research interests. Herein, the renovation of molecular chains and phase interface of rABS was successfully achieved through simple melt-blending modification, in which the in-situ chain extension reaction was conducted between rABS and pyromellitic dianhydride (PMDA). PMDA acted as a chain extender with hydroxyl units. The modified rABS were characterized by Fourier transform infrared spectroscopy (FTIR), gel permeation chromatography (GPC), mechanical properties testing, scanning electron microscopy (SEM), and dynamic mechanical analysis (DMA). The results indicated that compared with rABS, the molecular weight, impact strength, tensile strength, storage modulus and loss modulus of modified rABS were apparently improved. Especially, when PMDA content was 0.9 wt%, the notch impact strength reached 15.9 kJ/m^2, which was 140% higher than that of rABS. Besides, the interface between polybutadiene (PB) phase and styrene-acrylonitril copolymer (SAN) phase was blurred and the compatibility between two phases became better. The aforementioned results revealed that rABS has been achieved with high-value recycling usage.

1. Introduction

Acrylonitrile-butadiene-styrene (ABS) is a thermoplastic polymer formed by reaction among the acrylonitrile (A), butadiene (B) and styrene (S) [1]. Over the past few decades, ABS resin has been widely used in various fields such as electronics, automobiles, building materials and other industries [2] because of its excellent comprehensive performance, convenient processing and molding [3]. However, the aforementioned usages increasingly produced a large number of wasted ABS plastics [4]. Some traditional waste plastics processing methods, such as incineration and landfill, can cause serious environmental pollution and waste of resources [5–9]. Therefore, high value recycling of waste plastics is becoming urgently important [10,11].

During the processing and using processes, certain degradation of ABS resins decreased both molecular weight and mechanical properties because the carbon-carbon double bonds in the butadiene (B) phase were broken and produced oxygen containing groups such as carbonyl and hydroxyl, which could cause two-phase separation and poor compatibility in the polymer matrix [12–17]. In the conventional regeneration method, the recycled ABS resins achieved high-value recycling usage through adding a large number of polymer additives such as styrene-ethylene/butylenes-styrene (SEBS) and polyamide (PA) with high strength or high toughness [18–20]. These modifiers could only improve certain performances such as toughness, while led to the loss of material strength [19]. Meanwhile, a lower dosage of modifier had

* Corresponding author.
** Corresponding author.
E-mail addresses: liyingchun@126.com (Y. Li), zguo10@utk.edu (Z. Guo).
[1] contributed equally and should be treated as the co-first author.

http://dx.doi.org/10.1016/j.polymer.2017.07.042
0032-3861/

difficulty to give a significant improvement on the mechanical properties of ABS resins, however, a higher loading would cause high cost. More importantly, the physical blending could not achieve the renovation of molecular chains of rABS. Therefore, covalent modification of rABS resin is meaningful for the improvement of both molecular weight and mechanical properties.

Previous studies on the chain extension of rABS were focused on the carboxyl groups produced by the degradation of ABS, and the carboxyl type chain extenders such as epoxy resin [12] and oxazoline [21] were added. Pyromellitic dianhydride (PMDA) as a repair agent is a new type of chain extender. Up to now, PMDA was mainly used in the research of polyethylene terephthalate (PET) chain extension modification. The reaction between anhydride groups in PMDA and hydroxyl groups in PET resulted in the formation of ester groups, therefore, the PET molecular chains were connected by PMDA [22]. The research results showed that PMDA had some good effects on the chain extension of PET, for example, the length of molecular chains was increased, however, the viscosity was also increased [23,24]. Besides, Meng et al. found that the thermal degradation temperature of polylactide/clay nanocomposites was increased with the addition of PMDA since the polylactide in the clay nanocomposites was chain extended by PMDA, and the molecular chains of polylactide were increased with the addition of PMDA [25]. Although the hydroxyl groups can be produced in the degradation process of ABS and have potential to be used with PMDA for chain extension, the modification of rABS by PMDA has not been reported yet.

In this work, pyromellitic dianhydride (PMDA) was used as a chain extender with hydroxyl units to covalently modify rABS resin through a simple melt-blending process. The reparation effects of PMDA on rABS were studied in terms of chemical structure, molecular weight, mechanical properties, morphology and dynamic mechanical properties via Fourier transform infrared spectroscopy (FTIR), gel permeation chromatography (GPC), mechanical properties testing, scanning electron microscopy (SEM), and dynamic mechanical analysis (DMA). The renovation of molecular chains and phase interface of rABS was achieved and the renovation mechanisms were proposed as well.

2. Experimental

2.1. Materials

rABS was provided by Shundexin Environmental Protection Resources Utilization (Foshan, China). The chain extender PMDA (yellowish solid powder, melting point: 286 °C) was purchased from Hubei Kangbaotai Chemical Product Co. Ltd (Hubei, China). Tetrahydrofuran (THF) was provided by Tianjin kwangfu Fine Chemical Industry Research Institute. All the chemicals were used as received without any further treatments.

2.2. Preparation of PMDA/rABS composites

The samples were dried in a vacuum oven at 80 °C for rABS and 40 °C for PMDA for a period of 8 h before extrusion. And then rABS/PMDA was blended in an internal mixer (model XSM-1/70, Shanghai KCCK Co. Ltd., China) with a rotor speed of 60 rpm and at 180 °C. The reactive extrusion of the blends was carried out through a co-rotating twin-screw extruder containing gas bents and a vacuum system (SHJ-36, Chengmeng Equipment Co. Ltd, Nanjing, China). The accurate formulations are summarized in Table 1. The working temperature of extruder was kept in the range of 210–230 °C with a rotating speed of 75 rpm. Then the blends were injection molded through an injection-molding machine (JH600, Weidaliyuan Machinery Co. Ltd, Zhangjiagang, China). The temperature of injection-molding machine was kept in the range of 220–230 °C. The specimen with different shapes (dumbbell for tensile test; and rectangle for DMA test and notched rectangle for impact test) were obtained from the injection-molding. The notch for the injected molded rectangular sample was prepared by Notch Sampling Machine (Model: JC-3004, Jiangdu Jingcheng Testing Instrument Co., Ltd.).

Table 1
Compounding formulations of various rABS/PMDA ratios.

Ingredient	Blends					
	No.1	No.2	No.3	No.4	No.5	No.6
rABS	100	100	100	100	100	100
PMDA(wt%)	0	0.3	0.6	0.9	1.2	1.5

2.3. Characterizations

2.3.1. Fourier transform infrared spectroscopy (FT-IR)

The spectra of the rABS and rABS/PMDA samples were recorded on a Bruker Tensor 27 spectrometer (Bruker Optik GmbH, Madrid, Spain) in the range from 500 to 4000 cm^{-1} with a resolution of 4 cm^{-1}. All the samples were vacuum dried at 80 °C for 8 h before testing. Then, dry KBr was used to press the sample. The quantity ratio of KBr and sample was about 100:1.

2.3.2. Gel permeation chromatography (GPC)

The rABS and chain-extended rABS were grounded to powders (about 1.5 mg), and then dissolved in 1 mL THF, respectively. The solutions obtained were injected at a flow rate of 1 mL/min into a gel permeation chromatography instrument (Waters 515, Waters Corporation, Milford, USA) for test after 12 h at 25 °C.

2.3.3. Mechanical properties

Dumbbell shaped specimens of the rABS and chain-extended rABS were prepared for tensile testing. The tensile testing was performed at room temperature according to GB/T1040-92 using a universal testing machine (SANS CMT6104, Xinsansi Material Detection Co. Ltd, Shenzhen, China). The crosshead speed was 50 mm/min. The notch impact strength was tested by Izod impact tester (XJU-22, Chengde Precision Tester Co. Ltd, Chengde, China) according to GB/T184-89. The range of impact strength of rABS plastic used in this experiment was approximate between 5 and 20 kJ/m^2. The cross-section area of the specimen used in this experiment was 32 mm [2]. Thus, the absorbed energy was at 0.16–0.64 J. Finally, the test hammer with an energy of 1 J was selected for the test. The ultimate tensile strength, elongation at break and impact strength were averaged over at least five specimens.

2.3.4. Scanning electron microscopy (SEM)

The morphologies of the fracture surface of rABS and chain-extended rABS were examined by a Focused Ion Beam Scanning Electron Microscope (DB235, FEI Co. Ltd, Hillsboro, USA). The scanning voltage was 5 kV. The cross-section of dumbbell shaped specimens was gold-coated prior to the observations for better imaging.

2.3.5. Dynamic mechanical analysis (DMA)

The dynamic mechanical properties of rABS and chain-extended rABS were measured using dynamic mechanical analyzer (DMA800, Perkin Elmer Corporation, Waltham Massachusetts, USA) at a strain of 0.01% and a frequency of 1 Hz. Small tension-molded samples with dimensions of 9 × 4 × 2 mm were used for

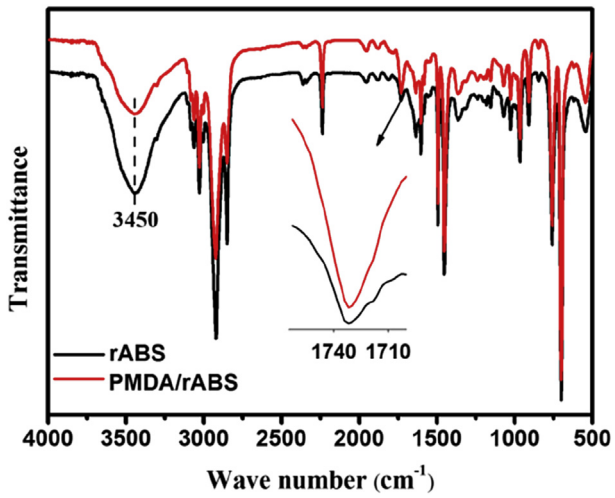

Fig. 1. The FT-IR spectra of rABS and PMDA/rABS, inset is the amplified part of the peak at 1735 cm^{-1}.

testing in a temperature range from −100 to 120 °C and at a heating rate of 3 °C/min.

3. Results and discussion

3.1. FTIR spectroscopy analysis

Fig. 1 shows the FT-IR spectrum of rABS. The observed strong peak at 3450 cm^{-1} was ascribed to the vibrational absorption of hydroxyl groups [26]. However, the hydroxyl peak in the PMDA(0.9 wt%)/rABS composites was weakened obviously, indicating that the hydroxyl groups were consumed by the anhydride functional groups during the chain-extension reaction. Similarly, the peak at 1735 cm^{-1} arising from the vibrational absorption of carbonyl ester groups [27] in the PMDA(0.9 wt%)/rABS composites was apparently stronger than that of the rABS resin. The resultant increased content of ester carbonyl indicated that the chain reaction between PMDA and rABS occurred. The reaction mechanisms of the ester formation are shown in Scheme 1 to Scheme 4 (The working temperature was kept in the range of 210–230 °C). Scheme 1 and Scheme 2 are coupled reactions. Scheme 3 and Scheme 4 are branching reaction. All of the possible reactions involve the ester formation, consistent with the results of infrared analysis. Similar reactions have been observed in the recently reported polymer composites [28–30].

3.2. Molecular weight

The molecular weight and molecular weight distribution of rABS, PMDA (0.9 wt%)/rABS and new ABS are showed in Table 2. Compared with rABS, the number-average molecular weight (Mn) and weight-average molecular weight (Mw) of PMDA (0.9 wt %)/rABS are increased by 134% and 33%, respectively, while polydispersity decreases from 5.35 to 3.03, which are closer to the values of new ABS (2.79, Table 2). The aforementioned results sufficiently indicate that the chain extension reaction between PMDA and rABS occurred, thus more broken molecular chains were connected and then effectively increased the molecular weight.

3.3. Mechanical properties

Fig. 2 shows the influence of PMDA content on the impact strength and tensile strength of rABS. Clearly, with the increase of PMDA, the impact strength and tensile strength of ABS are significantly increased. Especially, when the content of PMDA is 0.9 wt%, the impact strength of chain-extended rABS reaches the maximum of 15.9 kJ/m^2, which is 140% higher than that of rABS (6.7 kJ/m^2, Fig. 2). This is probably because the increased PMDA content promoted more chain extension reaction and improved the molecular weight of rABS. During the chain-extended reparation, the increase

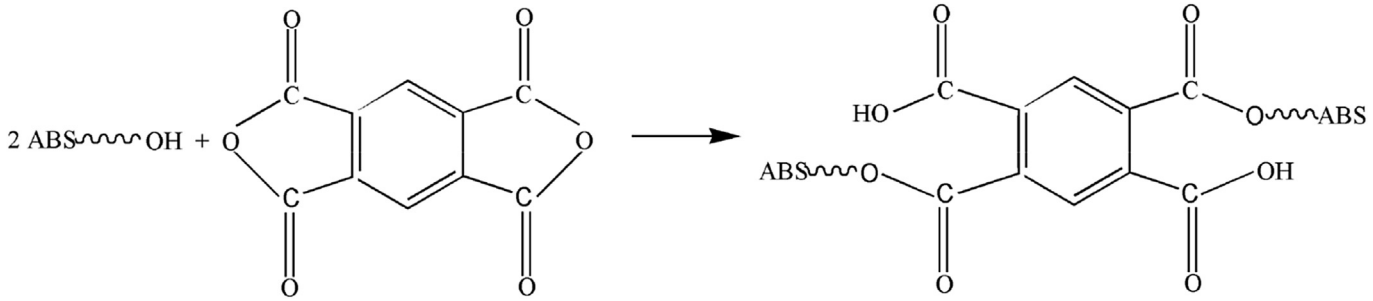

Scheme 1. Mechanism of the chain extension reaction between rABS and PMDA (coupled reaction).

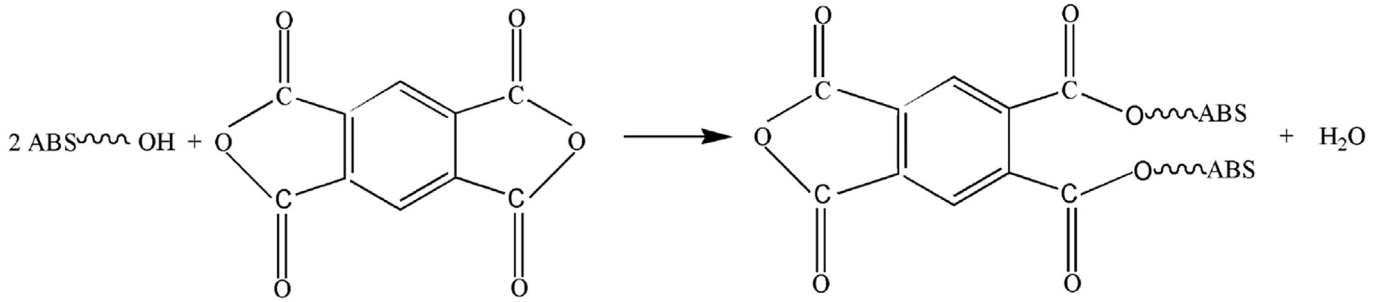

Scheme 2. Mechanism of the chain extension reaction between rABS and PMDA (coupled reaction).

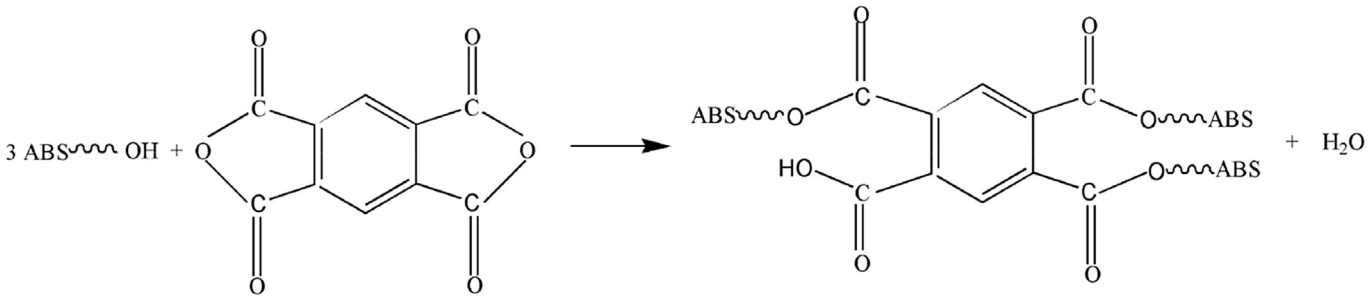

Scheme 3. Mechanism of the chain extension reaction between rABS and PMDA (branching reaction).

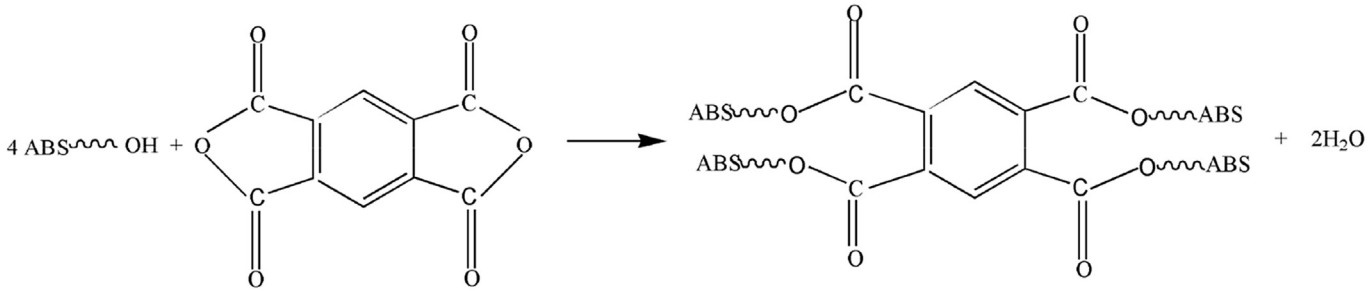

Scheme 4. Mechanism of the chain extension reaction between rABS and PMDA (branching reaction).

Table 2
Molecular weight and molecular weight distribution of polymer.

Specimen	Mn (g/mol)	Mw (g/mol)	Mw/Mn
rABS	8937	47830	5.35
PMDA(0.9 wt%)/rABS	20885	63268	3.03
ABS	22578	63042	2.79

of entanglements between the molecular chains will enhance the elastic contraction of the molecular chains and prohibit the molecules to slip. Therefore, with the impact of high speed load, the stress can be transmitted quickly, the ability to absorb the impact energy can be improved, so that the impact strength is increased and reaches the maximum [31]. Meanwhile, under the action of static load, the yield capacity of molecular chains in the load direction is increased. It is not easy to deform when the static load is applied, leading to an increased tensile strength.

Fig. 3 shows the influence of PMDA content on the elongation at break of rABS. The elongation at break is increasing with increasing the PMDA, illustrating that the increase of molecular chains brings more flexibility to the resin matrix. The elongation at break reflects the ability of large deformation of a material and is related to the strength of entire molecular chains and the ability of the molecular chain to move [32]. The impact strength and the elongation at break together characterize the toughness [33]. When the content of PMDA is 0.9 wt%, both the strength and elongation at break reach the maximum, its toughness is the highest.

3.4. Morphology of the fracture surface

Fig. 4 shows the morphology of the fractured surfaces of rABS and PMDA (0.9 wt%)/rABS. Many bare PB particles and holes left by PB particles [34] are obviously observed in the fractured surfaces of rABS (Fig. 4a), indicating that the interface separation between PB phase and SAN phase is obvious. When subjected to external forces, the flaws of rABS will be extended along the phase interface and

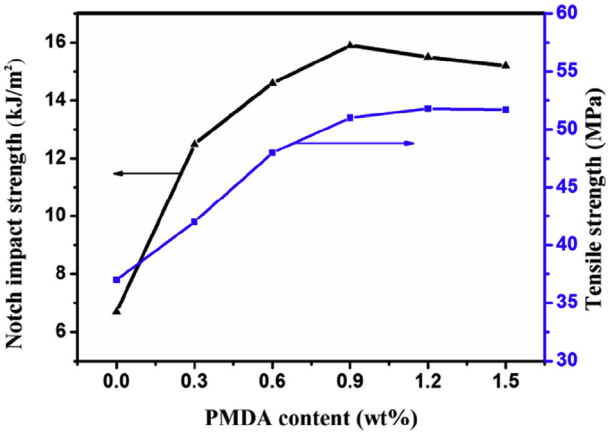

Fig. 2. Notch impact strengths and tensile strengths of the PMDA/rABS.

break the materials, thus the impact strength is reduced. Compared with rABS, the fractured interfaces of PMDA (0.9 wt%)/rABS with fibrillar structure [35] become more blurred (Fig. 4b), indicating that the renovation of molecular chains obviously improves the interface binding force between PB phase and SAN phase and achieves the phase interface reparation. This is probably because the broken PB was effectively repaired by PMDA and the PB-g-SAN grafting was also successfully repaired through the chain-extended reaction between PMDA and rABS. The results of SEM show that the fracture mode of rABS changes from brittle fracture (Fig. 4a) to ductile fracture [36], (Fig. 4b) which is consistent with the test results of impact strength (Fig. 2).

3.5. Dynamic mechanical analysis

With the change of temperature and time, polymers will show both viscosity and elasticity. The storage modulus, loss modulus and glass transition temperature (T_g) of the material can be

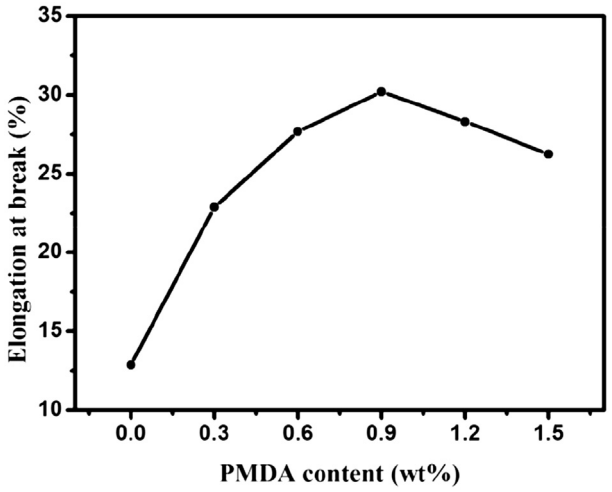

Fig. 3. Elongation at break of the PMDA/rABS with different PMA loadings.

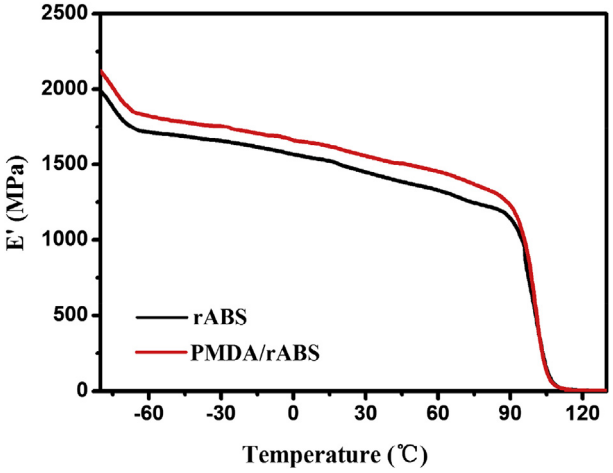

Fig. 5. Storage modulus (E′) curves of rABS and PMDA (0.9 wt%)/rABS.

obtained by DMA test. The storage modulus indicates the ability of a material to store elastic deformation energy. The loss modulus describes the energy dissipation of a material when it is deformed and it is a measure of energy loss [37]. The storage modulus curves of rABS and PMDA(0.9 wt%)/rABS vs temperature are plotted in Fig. 5. Owing to the energy dissipation, the storage modulus for the rABS and PMDA(0.9 wt%)/rABS is decreased with increasing the temperature. Compared with rABS, the storage modulus of PMDA/rABS is increased. From the point of molecular structure, the chemical bonding force of polymer molecules and the hydrogen bonds gives the polymer the ability to resist external forces [38]. After the chain-extended reaction, the molecular chains of rABS fracture are repaired and more chemical bonds are formed, therefore, the storage modulus increases.

Fig. 6 shows the curves of loss modulus of rABS and PMDA (0.9 wt%)/rABS vs the temperature. The peak in the low-temperature area (a) corresponds to the T_g of PB and the peak in the high-temperature area (b) corresponds to the T_g of SAN. Table 3 lists the T_g obtained from two peaks of loss modulus curve. Compared with rABS, the T_g of PB phase after chain extension was obviously increased, while the T_g of SAN phase almost kept constant. This is ascribed to the fact that the chain extender PMDA connects the broken PB, causing the molecular weight increased, and thus the molecular chain motion is more difficult and requires more energy, which causes the increased T_g [39]. Since there is no hydroxyl groups on SAN, it does not react with PMDA, and the T_g is almost unchanged. Besides, after extension with only 0.9 wt% PMDA, the T_g (−72.60 °C) of PB phase and the T_g (99.84 °C) of SAN phase are much closer than that (−76.73 °C) of PB phase and (100.09 °C) of SAN phase of rABS, this proves that the compatibility between PB and SAN is better [40]. And this is consistent with the observations of SEM (Fig. 4).

4. Conclusions

The renovation of molecular chain and phase interface of rABS was achieved through in situ chain extension reaction between rABS and PMDA. Compared with rABS, the mechanical properties of PMDA/rABS were obviously improved. Notably, when the PMDA content was 0.9 wt%, the notch impact strength reached 15.9 kJ/m^2, which was 140% higher than that of rABS. FT-IR and GPC test indicated that PMDA had an obvious chain extension effect on rABS, the molecular weight of PMDA/rABS was increased obviously and the molecular chain was repaired. The DMA test results proved that the storage modulus and loss modulus of PMDA/rABS blends were significantly higher than those of rABS, and the compatibility between PB and SAN was improved. The morphology of the fractured surface showed that the interface between PB phase and SAN phase was blurred and the fibrillar structure was observed, which indicated that the phase interface was repaired. This study provides a

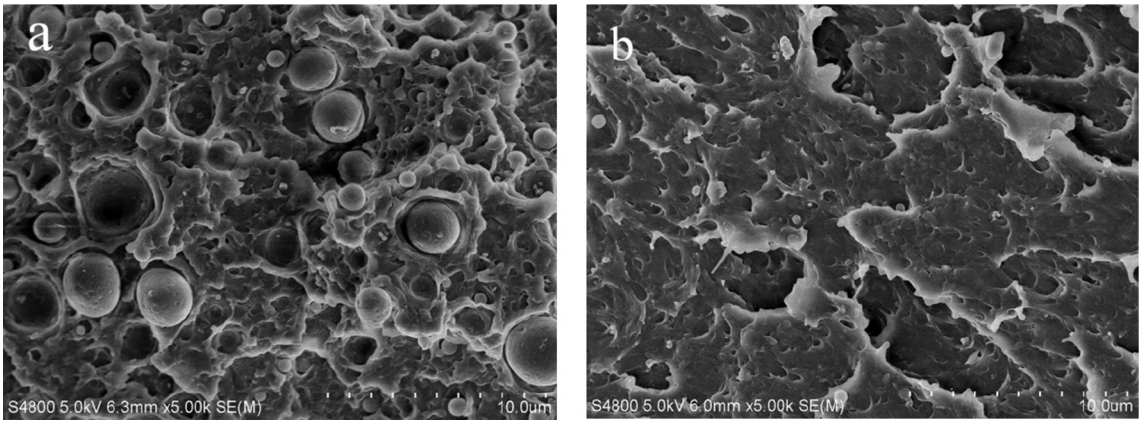

Fig. 4. SEM images of rABS and PMDA/rABS: (a) rABS; and (b) PMDA(0.9 wt%)/rABS.

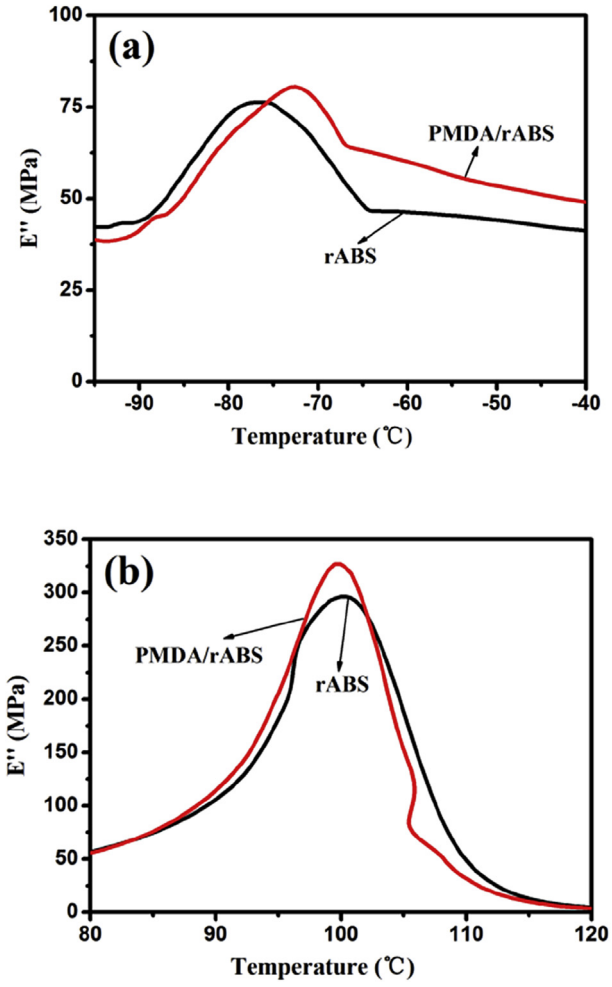

Fig. 6. Loss modulus (E″) curves of rABS and PMDA (0.9 wt%)/rABS (a) low-temperature zone (PB); (b) high-temperature zone (SAN).

Table 3
Glass transition temperatures of R- ABS and PMDA/rABS via DMA.

Specimen	Tg(°C)	
	PB	SAN
rABS	−76.73	100.09
PMDA(0.9 wt%)/rABS	−72.60	99.84

way to expand the usage of recycled plastics for multifunctional nanocomposites preparation with various fillers and different hosting polymer matrix [41–49].

References

[1] Y. Han, R. Lach, W. Grellmann, Effects of rubber content and temperature on unstable fracture behavior in ABS materials with different particle sizes, J. Appl. Polym. Sci. 79 (2001) 9–20.
[2] R. Balarta, D. García, M.D. Salvador, Recycling of ABS and PC from electrical and electronic waste. Effect of miscibility and previous degradation on final performance of industrial blends, Eur. Polym. J. 9 (2005) 2150–2160.
[3] P. Tarantili, A. Mitsakaki, M. Petoussi, Processing and properties of engineering plastics recycled from waste electrical and electronic equipment (WEEE), Polym. Degrad. Stab. 95 (2010) 405–410.
[4] P.A. Tarantili, Mitsakaki AN and Petoussi MA. Processing and properties of engineering plastics recycled from waste electrical and electronic equipment (WEEE), Polym. Degrad. Stab. 95 (2010) 405–410.
[5] B.H. Robinson, E-waste: an assessment of global production and environmental impacts, Sci. Total. Environ. 408 (2009) 183.
[6] H.G. Ni, E.Y. Zeng, Law enforcement and global collaboration are the keys to containing e-waste tsunami in China, Environ. Sci. Tech. 43 (2009) 3991–3994.
[7] J. Zhu, S. Wei, Y. Li, et al., Comprehensive and sustainable recycling of polymer nanocomposites, J. Mater. Chem. 21 (2011) 16239–16246.
[8] H. Gu, D. Ding, P. Sameer, et al., Microwave assisted formation of magnetic core-shell carbon nanostructure, ECS Solid. State. Lett. 2 (2013) M65–M68.
[9] J. Zhu, S. Pallavkar, M. Chen, et al., Magnetic carbon nanostructures: microwave energy-assisted pyrolysis vs conventional pyrolysis, Chem. Comm 49 (2013) 258–260.
[10] I.R. Cristian, B. Ilie, Waste electrical and electrical equipment (WEEE): a threat in the future, Metal. Int. 13 (2008) 12–17.
[11] B.B. Ramesh, A.K. Parande, B.C. Ahmed, Electrical and electrical waste:a global environmental problem, Waste manage. Res. 25 (2007) 307–318.
[12] J.C. Lee, H.T. Song, J.M. Yoo, Present status of the recycling of waste electrical and electronic equipment in Korea, Resour. Conserv. Recy 50 (2007) 380–397.
[13] Z. Sun, Z. Shen, X. Zhang, et al., Co-recycling of acrylonitrile–butadiene–styrene waste plastic and nonmetal particles from waste printed circuit boards to manufacture reproduction composites, Environ. Technol. 36 (2015) 160–168.
[14] J. Wang, Y.C. Li, J.F. Song, et al., Recycling of acrylonitrile-buta-diene-styrene (ABS) copolymers from waste electrical and electronic equipment(WEEE), through using an epoxy-based chain extender, Polym. Degrad. Stab. 112 (2015) 167–174.
[15] J.G. Bokria, S. Schlick, Spatial effects in the photodegradation of poly (acrylonitrile–butadiene–styrene): a study by ATR-FTIR, Polymer 43 (2002) 3239–3246.
[16] R.M. Santos, G.L. Botelho, A.V. Machado, Artificial and natural weathering of ABS, J. Appl. Polym. Sci. 116 (2010) 2005–2014.
[17] A. Arostegui, M. Sarrionandia, J. Aurrekoetxea, et al., Effect of dissolution-based recycling on the degradation and the mechanical properties of acrylonitrile–butadiene–styrene copolymer, Polym. Degrad. Stab. 91 (2006) 2768–2774.
[18] R.P. Singh, A.V. Prasad, S.S. Solanky, The oxidative degradation of styrenic copolymers: a comparison of photoproducts formation under natural and accelerated conditions, J. Appl. Polym. Sci. 85 (2002) 1676–1682.
[19] R.M. Santos, G.L. Botelho, C. Cramez, et al., Outdoor and accelerated weathering of acrylonitrile-butadientyrene: a correlation study, Polym. Degrad. Stab. 98 (2013) 2111–2115.
[20] R. Scaffaro, L. Botta, D.G. Benedetto, Physical properties of virgin-recycled ABS blends: effect of post-consumer content and of reprocessing cycles, Eur. Polym. J. 48 (2012) 637–648.
[21] M.A. Peydro, F. Parres, J.E. Crespo, et al., Recovery of recycled acrylonitrile–butadiene–styrene, through mixing with styrene–ethylene/butylene–styrene, J. Mater. Process. Technol. 213 (2013) 1268–1283.
[22] B. Liu, H. Lei, Recycled acrylonitrilebutadienestyrene copolymer resin strengthened and toughened by an elastomer/inorganic nanoparticles complex, J. Appl. Polym. Sci. 128 (2013) 2458–2467.
[23] J. Wang, Y.C. Li, J.F. Song, et al., Characterization of chain-extended recycled acrylonitrile-butadiene-styrene plastics by 1, 3-pbo, Eng. Plast. Appl. 43 (2015) 6–10.
[24] N. Xing JJ,Jiang, L.I. Yong, et al., Study on the comparison of the tackifying modification of PET by epoxy resin and quaternary anhydride, Chem. Adhes. 35 (2013) 24–28.
[25] A. Firas, D. Fugen, K. Edward, Recycled poly(ethylene terephthalate) chain extension by a reactive extrusion process, Polym. Eng. Sci. 44 (2010) 1579–1587.
[26] L. Incarnato, P. Scarfato, L.D. Maio, et al., Structure and rheology of recycled PET modified by reactive extrusion, Polymer 41 (2000) 6825–6831.
[27] Q. Meng, M.C. Heuzey, P.J. Carreau, Control of thermal degradation of polylactide/clay nanocomposites during melt processing by chain extension reaction, Polym. Degrad. Stabil. 97 (2012) 2010–2020.
[28] Y. Israeli, J. Lacoste, J. Lemaire, et al., Photo- and thermoinitiated oxidation of high-impact polystyrene. I. Characterization by FT-IR spectroscopy, J. Polym. Sci. Part A Polym. Chem. 32 (1994) 485–493.
[29] H. Horchani, M. Chaâbouni, Y. Gargouri, et al., Solvent-free lipase-catalyzed synthesis of long-chain starch esters using microwave heating: optimization by response surface methodology, Carbohydr. Polym. 79 (2010) 466–474.
[30] Y.J. Sun, G.H. Hu, M. Lambla, et al., In situ compatibilization of polypropylene and poly (butylene terephthalate) polymer blends by one-step reactive extrusion, Polymer 37 (1996) 4119–4127.
[31] G.H. Hu, G.T. Lindt, Monoesterification of styrene maleic anhydride copolymers with alcohols in ethyl benzene: catalysis and kinetics, J. Polym. Sci. Part A Polym. Chem. 31 (1993) 691–700.
[32] Y. Liu, N. Li, M. Run, Toughening poly (trimethylene terephthalate) by maleinized acrylonitrile-butadiene-styrene, Macromolecules 9 (2013) 91–101.
[33] H.Y. Liao, G.L. Tao, Impact strength and flow melt flow rate of high density polyethylene melts, Polym. Mater. Sci. Eng. 7 (2013) 72–75.
[34] P. Wang, Y. Li, M. He, et al., Chain extension modification of recycled high impact polystyrene with oxazoline, Polym. Mater. Sci. Eng. 31 (2015) 77–82.
[35] J. Wang, Y. Li, J. Song, et al., Characterization of chain-extended recycled acrylonitrile-butadiene-styrene plastics by 1,3–pbo, Eng. Plast. Appl. 6 (2015) 6–10.
[36] K.K. Ka, S. Srivastava, A. Rahaman, et al., Acrylonitrile-butadiene-styrene nanocomposites filled with nanosized alumina, Polym. Compos. 29 (2010)

489–499.
[37] X. Liu, Application of dynamic mechanical thermal analysis on polymer material, Eng. Plast. Appl. 38 (2010) 84–86.
[38] B. Wang, S. Sun, An investigation on the influence of molecular structure upon dynamic mechanical properties of polymer materials, Dev. App. Mater 2 (2005) 109–118.
[39] H.B. Gu, C. Mao, C.B. Liang, et al., A low loading of grafted thermoplastic polystyrene strengthens and toughens transparent epoxy composites, J. Mater. Chem. C 5 (2017) 4275–4285.
[40] J.E. Robertson, T.C. Ward, A.J. Hill, Thermal, mechanical, physical, and transport properties of blends of novel oligomer and thermoplastic polysulfone, Polymer 16 (2000) 6251–6262.
[41](a) Z. Sun, L. Zhang, F. Dang, et al., Experimental and simulation understanding of morphology controlled barium titanate nanoparticles under Co-adsorption of surfactants, CrystEngComm 19 (2017) 3288–3298;
(b) L. Zhang, W. Yu, C. Han, et al., Large scale synthesis of heterostructured electrospun TiO_2/SnO_2 nanofibers with an enhanced photocatalytic activity, J. Electrochem. Soc. (2017), http://dx.doi.org/10.1149/2.1531709jes in press.
[42] C. Wang, Y. Wu, Y. Li, et al., Flame retardant rigid polyurethane Foam with A Phosphorus-nitrogen single intumescent flame retardant, Polym. Adv. Technol. (2017), http://dx.doi.org/10.1002/pat.4105.
[43](a) Y. Zheng, Y. Zheng, S. Yang, et al., Esterification synthesis of ethyl oleate catalyzed by Brønsted acid-surfactant-combined ionic liquid, Green. Chem. Lett. Rev. 10 (2017) 202–209;
(b) W. Yang, X. Wang, J. Li, et al., Polyoxymethylene/ethylene butylacrylate copolymer/ethylene-methyl acrylate-glycidyl methacrylate ternary blends, Polym. Eng. Sci. (2017), http://dx.doi.org/10.1002/pen.24675.
[44] J. Guo, H. Song, H. Liu, et al., Polypyrrole-interface-functionalized nanomagnetite epoxy nanocomposites as electromagnetic wave absorber with enhanced flame retardancy, J. Mater. Chem. C 5 (2017) 5334–5344.
[45](a) X. Cao, X. Wei, G. Li, et al., Strain sensing behaviors of epoxy nanocomposites with carbon nanotubes under cyclic deformation, Polymer 112 (2017) 1–9;
(b) Q. Hu, D. Sun, Y. Ma, et al., Conductive polyaniline enhanced methane production from anaerobic wastewater treatment, Polymer 120 (2017) 236–243.
[46] T. Gong, M. Liu, H. Liu, et al., Selective distribution and migration of carbon nanotubes enhanced electrical and mechanical performances in polyolefin elastomers, Polymer 110 (2017) 1–11.
[47] X. Guan, G. Zheng, K. Dai, et al., Carbon nanotubes-adsorbed electrospun PA66 nanofiber bundles with improved conductivity and robust flexibility, ACS Appl. Mater. Inter 8 (2016) 14150–14159.
[48] H. Liu, M. Dong, W. Huang, et al., Lightweight conductive graphene/thermoplastic polyurethane foams with ultrahigh compressibility for piezoresistive sensing, J. Mater. Chem. C 5 (2017) 73–83.
[49] L.C. Jia, Y.K. Li, D.X. Yan, Flexible and efficient electromagnetic interference shielding materials from ground tire rubber, Carbon 121 (2017) 267–273.